
Kill it with FIRE: On Leveraging Latent Space Directions for Runtime Backdoor Mitigation in Deep Neural Networks

Enrico Ahlers¹ Daniel Passon¹ Yannic Noller² Lars Grunske¹

Abstract

Machine learning models are increasingly present in our everyday lives; as a result, they become targets of adversarial attackers seeking to manipulate the systems we interact with. A well-known vulnerability is a *backdoor* introduced into a neural network by poisoned training data or a malicious training process. Backdoors can be used to induce unwanted behavior by including a certain trigger in the input. Existing mitigations filter training data, modify the model, or perform expensive input modifications on samples. If a vulnerable model has already been deployed, however, those strategies are either ineffective or inefficient. To address this gap, we propose our inference-time backdoor mitigation approach called *FIRE* (*Feature-space Inference-time REpair*). We hypothesize that a trigger induces structured and repeatable changes in the model’s internal representation. We view the trigger as *directions* in the latent spaces between layers that can be applied in reverse to correct the inference mechanism. Therefore, we turn the backdoored model against itself by manipulating its latent representations and moving a poisoned sample’s features along the backdoor directions to neutralize the trigger. Our evaluation shows that *FIRE* has low computational overhead and outperforms current runtime mitigations on image benchmarks across various attacks, datasets, and network architectures.

1. Introduction

Deep neural networks are widely used across real-world disciplines such as computer vision (Krizhevsky et al., 2012; Simonyan et al., 2014), autonomous driving (Tampuu et al., 2022), healthcare (Litjens et al., 2017) and finance (Mienye et al., 2024). Their deployment in safety- and security-

critical applications, however, has raised significant concerns regarding their robustness and trustworthiness, particularly in adversarial settings.

One prominent threat to the integrity of deep neural networks is the presence of backdoors. Backdoor attacks deliberately manipulate the training data or training procedure by embedding hidden triggers that cause the model to exhibit attacker-chosen behavior at inference time (Gu et al., 2019b; Zeng et al., 2023; Mengara et al., 2024; Li et al., 2026; Wu et al., 2026). While the model performs normally on benign inputs, the presence of a specific trigger can reliably induce misclassification into a target label. Due to their stealthy nature and high attack success rates, backdoors pose a serious risk in scenarios where training is outsourced, or pre-trained models are obtained from untrusted sources.

As a result, substantial research effort has been devoted to the detection and mitigation of backdoors in neural networks. Existing defenses can be categorized into pre-training, training, post-training, deployment, and inference-time approaches (Wu et al., 2026). Pre-training and training-time defenses require access to the data or training process and are therefore inapplicable once a model has been deployed, while post-training and deployment-time methods often involve modifying model weights or parameters, or rejecting suspicious inputs.

In this work, we focus on inference-time defenses, which aim to mitigate backdoor behavior during runtime without retraining, finetuning or modifying the weights of the model. Existing inference-time approaches often either act as firewalls that detect and reject suspected inputs or attempt to remove triggers through input modification. A key limitation of firewall-style defenses is that simply discarding flagged samples is not acceptable in many safety-critical settings where a decision is required. For example, if a backdoored traffic sign classifier encounters a traffic sign with an adversarial sticker, the system cannot ignore the sign; it must recover the correct prediction to ensure safe behavior. Existing input modification methods can sometimes enable such correction, but they often incur substantial computational cost and are slow at inference time (Shi et al., 2023; Yang et al., 2024). These limitations motivate lightweight inference-time mitigation methods that correct poisoned

¹Humboldt University of Berlin, Germany ²Ruhr University Bochum, Germany. Correspondence to: Enrico Ahlers <enrico.philip.ahlers@hu-berlin.de>.

predictions without modifying the model parameters.

In our approach, we take a different perspective by analyzing the internal latent representations of backdoored models. We show that examining multiple latent spaces provides valuable insight into how backdoors manifest within the network. In particular, we study the directions induced by the trigger in latent space and discuss approaches for identifying these directions. Our analysis reveals that poisoned samples align along consistent directions in certain latent spaces of the network. The particular latent spaces in which this behavior emerges depend on the attack method, model architecture, and dataset.

Building on this observation, we propose a novel runtime backdoor mitigation method that leverages the latent directions associated with the trigger. Instead of modifying the input image or changing the model parameters, our approach operates directly on the latent representation of the input during inference. By moving the representation along the identified backdoor directions, the poisoned sample is effectively purified, restoring the correct prediction. This procedure does not require expensive optimization or access to large clean datasets and can be applied at runtime without altering the network. Owing to its low computational overhead, the mitigation can be updated online during inference, allowing the estimation of the backdoor directions to improve progressively as new samples are processed.

Extensive experiments across multiple datasets and network architectures demonstrate that the proposed method consistently outperforms existing runtime mitigation techniques. These results suggest that latent-space analysis offers a powerful and practical avenue for understanding and defending against backdoor attacks, enabling efficient and non-intrusive mitigation in deployed deep learning systems.

2. Preliminaries and Related Work

2.1. Backdoor Attack

Backdoor attacks constitute a class of training-time attacks in which an adversary embeds hidden triggers into a model by poisoning the training data or manipulating the training procedure (Gu et al., 2019a; Bagdasaryan et al., 2020; Xi et al., 2021). When the trigger is present at inference time, the model reliably produces an attacker-chosen target prediction while maintaining high accuracy on clean inputs (Nguyen & Tran, 2020b). Backdoor attacks can be highly effective and generalize across modalities (e.g., vision, speech, text, and reinforcement learning) while evading standard validation, including via clean-label poisoning, adaptive/input-aware triggers, and transfer- or pretraining-based injection (Turner et al., 2019; Nguyen & Tran, 2020a; Kurita et al., 2020; Zhai et al., 2021; Xu et al., 2024).

2.2. Backdoor Mitigation

In response, a wide range of defense mechanisms has been proposed across different stages of the machine learning pipeline (Jin et al., 2025; Wu et al., 2026). Among post-training defenses, existing methods typically require either (i) training additional components (e.g., auxiliary modules or purification generators) (Doan et al., 2020; Zhu et al., 2023; Al Kader Hammoud et al., 2023; Li et al., 2023; Huang et al., 2023; Xu et al., 2023; Luo et al., 2025; Zhu et al., 2025; Chen et al., 2025), (ii) solving expensive non-trivial optimization problems at deployment (e.g., UNIT (Cheng et al., 2024) and MMAC (Wang et al., 2024)), or (iii) modifying the deployed model via parameter updates (Li et al., 2020; Usman et al., 2021), pruning (Liu et al., 2018), or unlearning (Wang et al., 2019; 2022b). However, defenders often lack access to the required datasets or computational resources, motivating inference-time techniques.

Inference-time defenses are particularly relevant for deployed systems and include detection-based approaches, such as SentiNet (Chou et al., 2020) and STRIP (Gao et al., 2019), which aim to identify poisoned inputs and then discard suspicious samples. However, in settings like autonomous driving, abstention is infeasible, and the prediction must instead be corrected.

For inference-time correction, input-space purification methods have shown promising results. A lightweight baseline is ShrinkPad (Li et al., 2021), though diffusion-based purification can achieve higher accuracy. ZIP (Shi et al., 2023) applies a pretrained diffusion model entirely at test time, but is comparatively expensive at inference. In contrast, SampDetox (Yang et al., 2024) requires a domain-specific diffusion model, and BDFirewall (Li et al., 2025) additionally trains a U-Net on top of such a model, violating our *no-training* constraint. Other defenses further require mask localization and/or iterative inpainting optimization (Usman et al., 2022; Wei et al., 2023; May et al., 2023; Sun et al., 2025), which increases runtime cost and can depend on spatial trigger structure, which limits their applicability; BDMAE (Sun et al., 2025) is designed for localized triggers; Shi et al. show it breaks down on image-wide triggers, which our setting requires handling (2023).

2.3. Latent-Space Representations

We use *feature space* and *latent space* interchangeably to refer to intermediate representations in a deep neural network. A substantial body of work has shown that the latent spaces of deep neural networks encode rich semantic structure (Bank et al., 2023; Hu et al., 2023; Jebreel et al., 2024). In generative models, especially GANs, linear and non-linear directions in latent space have been shown to correspond to high-level semantic attributes, enabling controlled manipulation of generated images (Parihar et al., 2022). Similar

observations have been made for discriminative models, where internal representations capture class-relevant and concept-level information. Recent work demonstrates that attributes, styles, and semantic variations can often be isolated along specific latent directions, sometimes consistently across samples (Parihar et al., 2022). These findings suggest that latent spaces provide a meaningful and structured representation of input data. Importantly, prior analysis shows the backdoor signal is not guaranteed to be most separable in the final (commonly used) latent layer; the strongest benign-poisoned feature difference can occur at an earlier critical layer (Jebreel et al., 2024). This work builds on the insight that backdoor behavior is reflected in internal representations and leverages latent directions as a practical mechanism for inference-time backdoor mitigation.

To the best of our knowledge, *FIRE* is the first method to use latent-space representations for inference-time sample correction, leveraging them to update its correction as new samples arrive.

2.4. Network and Data Notation

Let a feed-forward neural network f be a composition of L layers

$$f = f_{L-1} \circ f_{L-2} \circ \cdots \circ f_0, \quad (1)$$

where each layer is a mapping between Euclidean spaces

$$f_\ell : \mathbb{R}^{d_{\ell-1}} \rightarrow \mathbb{R}^{d_\ell}, \quad \ell \in \{0, \dots, L-1\}, \quad (2)$$

with input dimension d_{-1} and output dimension d_{L-1} (e.g. logits). For any input $x \in \mathbb{R}^{d_{-1}}$, define the depth- ℓ latent map $h_\ell : \mathbb{R}^{d_{-1}} \rightarrow \mathbb{R}^{d_\ell}$ and the corresponding tail network $g_\ell : \mathbb{R}^{d_\ell} \rightarrow \mathbb{R}^{d_{L-1}}$ by

$$h_\ell = f_\ell \circ f_{\ell-1} \circ \cdots \circ f_0, \quad h_0 := f_0, \quad (3)$$

and

$$g_\ell := f_{L-1} \circ f_{L-2} \circ \cdots \circ f_{\ell+1}, \quad g_{L-1} := \text{id} \quad (4)$$

so that $f(x) = g_\ell(h_\ell(x))$ for all ℓ .

Clean and Poisoned Samples Let $\{x_i^{\text{clean}}\}_{i=1}^N$ be N clean samples in $\mathbb{R}^{d_{-1}}$. A *trigger injection operator* is a (possibly input-dependent) function $\mathcal{T} : \mathbb{R}^{d_{-1}} \rightarrow \mathbb{R}^{d_{-1}}$ that adds a trigger to an input. The poisoned counterpart is

$$x_i^{\text{pois}} := \mathcal{T}(x_i^{\text{clean}}). \quad (5)$$

Latent Displacements For each paired sample $(x_i^{\text{clean}}, x_i^{\text{pois}})$ we denote their representations after layer f_ℓ by

$$x_{i,\ell}^{\text{clean}} := h_\ell(x_i^{\text{clean}}) \in \mathbb{R}^{d_\ell}, \quad (6)$$

$$x_{i,\ell}^{\text{pois}} := h_\ell(x_i^{\text{pois}}) \in \mathbb{R}^{d_\ell}. \quad (7)$$

We then define the *sample-wise trigger displacement* in latent space after layer f_ℓ as

$$b_{i,\ell} := x_{i,\ell}^{\text{pois}} - x_{i,\ell}^{\text{clean}} \in \mathbb{R}^{d_\ell}. \quad (8)$$

Importantly, $b_{i,\ell}$ is allowed to depend on the sample index i and (implicitly) on the trigger mechanism \mathcal{T} ; i.e. displacements can vary across inputs and triggers.

3. Methodology

3.1. Intuition and Observations

Semantic manipulations can be captured as approximately linear directions in latent representations, as shown by FLAME (Parihar et al., 2022). Building on this perspective, we next estimate a *general* trigger that can be interpreted as an (approximately) linear direction in one or multiple latent spaces of the network.

In Eq. 8, we defined the *sample-wise* trigger displacement $b_{i,\ell}$. Empirically, we show that backdoored models often encode the individual displacements $b_{i,\ell}$ in a highly consistent manner in at least one latent space, i.e., these vectors exhibit strong alignment (or low-variance structure) across many samples. Based on this perspective, we introduce *FIRE* (*Feature-space Inference-time REpair*), an inference-time mitigation approach that corrects poisoned predictions by intervening directly in intermediate representations.

This observation is compatible with the hierarchical nature of learned representations: earlier layers tend to capture low-level and coarse visual primitives, while deeper layers represent increasingly complex and task-specific features (Zeiler & Fergus, 2014). Consequently, the latent space(s) in which a general trigger direction emerges depends on the trigger’s complexity: simple patterns may manifest as a consistent shift in earlier representations, whereas more structured triggers may only align in deeper latent spaces.

Once such a general direction has been identified, the trigger effect can be modeled as an additive component in latent space. This enables a simple repair operation: adding the direction applies the trigger in latent space, while subtracting it removes (or reduces) the trigger contribution before forwarding the corrected representation through the remaining network.

To summarize, *FIRE* is based on the hypothesis that backdoors induce a structured, repeatable displacement in latent space that becomes sufficiently coherent at some depth to be approximated by a linear direction.

3.2. Estimating the General Trigger Direction

We propose two strategies to obtain latent directions, depending on the defender’s knowledge; additional strategies

are provided in Appendix A.

Strategy 1: Paired Clean/Poisoned Samples If paired samples are available, i.e., we have access to both a clean and a corresponding poisoned version of the same underlying input, we can directly form pairs $(x_i^{\text{clean}}, x_i^{\text{pois}})$. If paired samples are not available, but the trigger injection operator \mathcal{T} is known (e.g., via trigger reconstruction), we can instead generate pairs by applying \mathcal{T} to clean inputs, as in Eq. 5. For a fixed candidate layer f_ℓ , we compute the sample-wise displacement in latent space,

$$b_{i,\ell} = h_\ell(x_i^{\text{pois}}) - h_\ell(x_i^{\text{clean}}) \in \mathbb{R}^{d_\ell}, \quad (9)$$

which corresponds to Eq. 8. Repeating this for N pairs yields a general direction by averaging:

$$\hat{b}_\ell := \frac{1}{N} \sum_{i=1}^N b_{i,\ell} = \frac{1}{N} \sum_{i=1}^N (h_\ell(x_i^{\text{pois}}) - h_\ell(x_i^{\text{clean}})). \quad (10)$$

This estimator directly captures the dominant shared component of the per-sample displacements at layer f_ℓ .

Strategy 2: Unpaired Clean and Poisoned Sets (Unknown Trigger) with Image Augmentations In many settings, the trigger in input space is unknown, which makes it infeasible to construct paired samples. Instead, we assume access to an unpaired set of clean samples $\{x_i^{\text{clean}}\}_{i=1}^{N_c}$ and a set of poisoned samples $\{x_j^{\text{pois}}\}_{j=1}^{N_p}$ (not necessarily corresponding to the same underlying images). For a candidate layer f_ℓ , we compute empirical centroids in latent space,

$$\hat{\mu}_\ell^{\text{clean}} := \frac{1}{N_c} \sum_{i=1}^{N_c} h_\ell(x_i^{\text{clean}}), \quad (11)$$

$$\hat{\mu}_\ell^{\text{pois}} := \frac{1}{N_p} \sum_{j=1}^{N_p} h_\ell(x_j^{\text{pois}}), \quad (12)$$

and define a centroid-difference of the trigger direction as

$$\hat{b}_\ell^{\text{diff}} := \hat{\mu}_\ell^{\text{pois}} - \hat{\mu}_\ell^{\text{clean}}. \quad (13)$$

If, after layer f_ℓ , poisoned representations exhibit an approximately consistent shift relative to clean ones, then $\hat{b}_\ell^{\text{diff}}$ averages out sample-specific variation across examples and leaves the common shift direction induced by the trigger.

Augmentation-based estimate Gao et al. report that backdoor-trigger features tend to be more fragile under image corruptions than genuine semantic features (2024). We exploit this by constructing pairs consisting of a poisoned input and an augmented copy of the same poisoned input. Let $\mathcal{A} : \mathbb{R}^{d-1} \rightarrow \mathbb{R}^{d-1}$ denote an augmentation/corruption operator (e.g., additive noise, blur, JPEG compression, random resizing/cropping), and define

$$x_i^{\text{pois},\text{aug}} := \mathcal{A}(x_i^{\text{pois}}). \quad (14)$$

For a candidate layer f_ℓ , we compute the sample-wise augmentation-induced displacement in latent space,

$$b_{i,\ell}^{\text{aug}} := h_\ell(x_i^{\text{pois}}) - h_\ell(x_i^{\text{pois},\text{aug}}) \in \mathbb{R}^{d_\ell}. \quad (15)$$

Under the assumption that semantic features are comparatively stable under \mathcal{A} while trigger-related features degrade disproportionately, $b_{i,\ell}^{\text{aug}}$ is dominated by the trigger change and thus serves as a proxy for the backdoor direction. Aggregating over N_p poisoned samples yields

$$\hat{b}_\ell^{\text{aug}} := \frac{1}{N_p} \sum_{i=1}^{N_p} b_{i,\ell}^{\text{aug}}. \quad (16)$$

Combined direction Finally, we combine the centroid-difference and augmentation-based estimates using trade-off parameter λ to obtain a single trigger direction at layer f_ℓ :

$$\hat{b}_\ell := \lambda \hat{b}_\ell^{\text{diff}} + (1 - \lambda) \hat{b}_\ell^{\text{aug}}, \quad \lambda \in [0, 1]. \quad (17)$$

3.3. Direction-Based Latent Repair

Given an estimated general trigger direction \hat{b}_ℓ at layer f_ℓ , we repair an input x by modifying its latent representation $x_\ell := h_\ell(x)$ such that the trigger contribution is reduced. Conceptually, we move x_ℓ in the opposite direction of \hat{b}_ℓ , i.e., we “subtract” the trigger component before forwarding the corrected representation through the tail network g_ℓ .

The repair operator subtracts the direction estimate,

$$\tilde{x}_\ell = \text{Rep}_\ell(x_\ell, \hat{b}_\ell, \alpha_\ell) := x_\ell - \alpha_\ell \hat{b}_\ell, \quad (18)$$

where $\alpha_\ell \in \mathbb{R}$ controls repair strength (typically $\alpha_\ell = 1$).

The repaired prediction is obtained by forwarding \tilde{x}_ℓ through the rest of the network, i.e., $y_{\text{rep}} = \arg \max g_\ell(\tilde{x}_\ell)$.

4. Empirical Study

We now empirically test the hypothesis from Section 3: in a backdoored network, the trigger induces a consistent, approximately linear displacement in latent space at certain depths. If such a direction can be identified, subtracting it at inference time should reduce the trigger effect and recover the clean prediction. A key focus is *layer dependence*: we analyze at which layers the displacement is sufficiently coherent for latent-space repair to be effective.

To isolate the effect of latent space selection from estimation noise, we construct $N = 100$ paired samples $(x_i^{\text{clean}}, x_i^{\text{pois}})$ by inserting known triggers in input space and estimate a direction \hat{b}_ℓ for each latent space using Strategy 1 (Eq. 10).

Configurations We evaluate on CIFAR-10 (Krizhevsky & Hinton, 2009) and GTSRB (Stallkamp et al., 2011) using PreActResNet classifiers (He et al., 2016) trained under a poisoning ratio of 10% across a range of backdoor

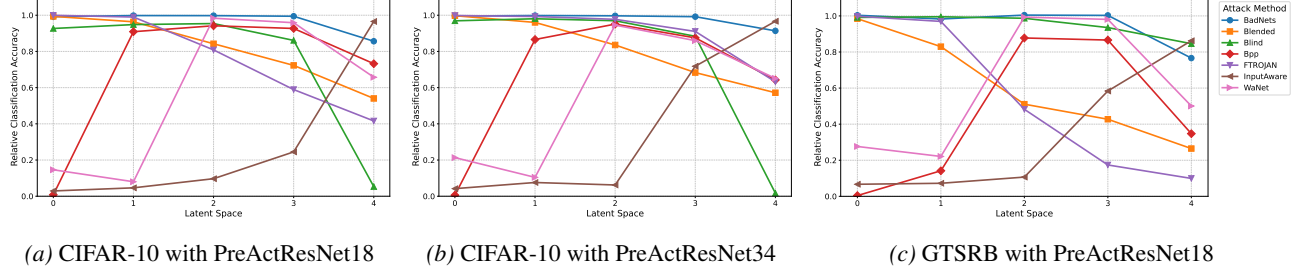


Figure 1. Mitigation performance when intervening *manually* at each latent space. The x-axis shows the selected latent space, while the y-axis shows the *relative* classification accuracy (%), i.e. the Poisoned Accuracy (PA) divided by the Clean Accuracy (CA) of the model.

attacks: BadNets (Gu et al., 2019a), Blended (Chen et al., 2017), Blind (Bagdasaryan & Shmatikov, 2021), Bpp (Wang et al., 2022c), FTROJAN (Wang et al., 2022a), InputAware (Nguyen & Tran, 2020a), and WaNet (Nguyen & Tran, 2020b). 5 latent spaces are used; one after the first convolutional layer, and one after each block.

We benchmark mitigation by intervening at each candidate latent space after layer f_ℓ . Concretely, for each ℓ we compute the repaired prediction

$$y_{\text{rep}}^{(\ell)}(x) = \arg \max g_\ell\left(\text{Rep}_\ell(h_\ell(x))\right), \quad (19)$$

and report the Poisoned Accuracy (PA, %), defined as the accuracy on poisoned inputs with respect to the ground-truth labels, as a function of ℓ .

Fig. 1 summarizes the resulting *relative* layer-wise performance distribution across attacks. The key takeaway is that repair is highly depth-dependent: certain attacks become reliably correctable only after the trigger effect emerges as a coherent displacement in deeper representations, while others admit effective repair in earlier latent spaces. Intuitively, different attacks introduce different trigger features (e.g., localized patches or full-image warps), and these features become separable and stable at different representational stages. For example, the WaNet attack can be best mitigated at latent space 2, while a mitigation at latent space 0 and 1 yields poor results. Notably, these preferred intervention depths are highly consistent across different datasets and model architectures, suggesting that the optimal depth is driven primarily by the backdoor attack mechanism, rather than dataset- or architecture-specific effects.

Tab. 1 reports the correction performance of poisoned images to their true labels at different latent spaces. Across all three dataset–architecture configurations, we observe consistently strong recovery of the true label in at least one latent space. In many cases, the PA after correction is close to the Clean Accuracy (CA). The lowest performance occurs for the InputAware attack on a PreActResNet18 on GTSRB, where PA reaches 84.1% compared to a CA of 97.51%, i.e., a gap of 13.41%. For over half of the configurations, we

identify a direction that recovers the true label within 1% of the CA.

Comparison to Prior Work Unlike Jebreel et al. (2024), who emphasize that backdoor effects become most distinctive in the *second half* of the network, we find that for *purification* the optimal intervention depth is often much earlier: attacks such as Blended and BadNets are best mitigated in early latent spaces, while others (e.g., InputAware) still prefer later layers. This supports the view that repair works best at the earliest depth where the trigger is already encoded as a stable shift, before salient image content is discarded by later representations.

5. Runtime Backdoor Mitigation

5.1. Threat Model and Deployment Setting

We consider a defense scenario in which a potentially backdoored model is already trained and deployed, and the defender must mitigate malicious behavior *during inference* under strict real-time constraints.

Attacker Capabilities The attacker has full control over the training pipeline. Concretely, the attacker can poison the training dataset and influence the training procedure itself, with the goal of implanting a backdoor into the resulting model. As in standard backdoor settings, the backdoored model behaves normally on benign inputs but, when a trigger is present, predicts an attacker-chosen target label with high probability.

Defender Capabilities The defender is assumed to have access to:

- A *small* set of clean reference samples (without triggers), denoted by $\mathcal{D}_{\text{clean}} = \{x_i\}_{i=1}^{N_c}$.
- Inference access to the deployed model $f = f_{L-1} \circ \dots \circ f_0$, including the ability to compute predictions $f(x)$ and to extract latent representations $h_\ell(x)$ for selected ℓ during a forward pass.

Table 1. Correction performance on 21 configurations, reporting Clean Accuracy (CA, %) and Poisoned Accuracy (PA, %) without defense, and Poisoned Accuracy (PA, %) with FIRE applied in different latent spaces. “Diff to CA” (%) indicates the difference between CA and PA (CA – PA) in the best-performing latent space.

CONFIGURATION	ATTACK	CA \uparrow	PA \uparrow	PA IN LATENT SPACE \uparrow					DIFF TO CA \downarrow
				0	1	2	3	4	
PREACTRESNET18 CIFAR-10	BADNETS	91.84	5.27	91.12	91.66	91.63	91.33	78.64	0.18
	BLENDENED	93.57	0.18	92.97	90.18	78.83	67.64	50.55	0.60
	BLIND	80.17	0.40	74.30	76.02	76.48	69.02	4.27	3.69
	BPP	90.99	0.39	0.72	82.71	85.70	84.34	66.62	5.29
	FTROJAN	93.56	0.00	93.52	92.63	75.64	55.13	38.91	0.04
	INPUTAWARE	91.28	2.54	2.66	4.24	8.84	22.36	88.13	3.15
	WANET	91.19	3.90	13.33	7.30	89.69	87.42	59.96	1.50
PREACTRESNET18 GTSRB	BADNETS	96.05	3.73	96.39	94.41	96.49	96.34	73.60	-0.44
	BLENDENED	97.05	0.27	95.56	80.52	49.57	41.47	25.70	1.49
	BLIND	57.28	41.23	56.81	57.02	56.54	53.58	48.47	0.27
	BPP	96.79	0.24	0.40	13.71	84.96	83.84	33.62	11.84
	FTROJAN	98.11	0.00	97.92	95.12	47.32	17.06	9.74	0.18
	INPUTAWARE	97.51	6.17	6.52	7.05	10.40	56.93	84.10	13.41
	WANET	96.80	7.06	26.75	21.40	96.14	94.94	48.45	0.66
PREACTRESNET34 CIFAR-10	BADNETS	92.47	4.31	92.06	92.30	92.17	91.73	84.49	0.17
	BLENDENED	94.04	0.21	93.79	90.30	78.58	64.25	53.78	0.25
	BLIND	89.36	0.03	86.60	87.62	86.64	78.96	1.52	1.74
	BPP	92.21	0.28	0.53	79.84	87.69	80.69	59.25	4.52
	FTROJAN	93.60	0.06	93.45	92.93	91.48	85.22	59.18	0.15
	INPUTAWARE	91.57	3.71	3.84	6.94	5.70	65.76	88.52	3.05
	WANET	90.15	9.74	19.24	9.40	85.22	77.49	58.69	4.93

However, the defender *cannot* assume access to the original training data, cannot modify model weights, and cannot afford computationally intensive procedures such as retraining, fine-tuning, or optimization-based purification at test time. The defense must therefore be a lightweight procedure implementable as an extension of the forward pass.

Runtime Input Stream At deployment, we consider a stream of flagged inputs $\{x_t\}_{t=1}^{\infty}$ that are treated as poisoned. Such a flagged stream can arise by filtering a larger, mostly clean deployment stream through an upstream backdoor-detection module (e.g., SCALE-UP (Guo et al., 2022) or related methods (Wu et al., 2026))¹. We assume the system cannot discard flagged inputs; in safety-critical settings, abstention may be infeasible and a prediction must be produced for every query. We therefore focus on *post-detection mitigation*: efficiently recovering correct predictions on flagged inputs, analogous to the streaming-style runtime repair setting discussed in ZIP (Shi et al., 2023).

Practical Motivation A canonical example is autonomous driving. Consider a backdoored traffic sign classifier deployed on a vehicle. If an attacker places a trigger (e.g., a small sticker) on a traffic sign, the classifier may output an incorrect label. The vehicle cannot ignore the sign or stop to run expensive defenses; it must instead correct

¹We study the impact of imperfect detectors in Appendix D.

the prediction *immediately* to ensure safe behavior. This motivates a defense that operates directly on internal representations during a forward pass, without updating model weights.

5.2. Defense Procedure

We now instantiate the methodology from Section 3.2 and 3.3 for the real-time threat model in Section 5.1. Alg. 1 summarizes the full streaming defense: it maintains online estimates of a trigger direction in multiple candidate latent spaces and applies repair at the earliest latent space that changes the model’s prediction on the current input.

Initialization As illustrated in Fig. 2, we first compute a clean reference statistic for each candidate latent space after $f_{\ell}, \ell \in \mathcal{L}$, namely the clean centroid $\hat{\mu}_{\ell}^{\text{clean}}$ (Eq. 11). This provides a layer-wise baseline that online estimates are compared to.

Online Runtime Loop At runtime, the defense processes a stream of poisoned inputs. For each input, it first records the model’s unmitigated prediction and then evaluates candidate latent spaces in ascending order. At each latent space, the defense (i) updates its current estimate of the trigger direction using the arriving sample (Eq. 13), (ii) repairs the corresponding latent representation (Eq. 18), and (iii) checks whether this repaired representation alters the pre-

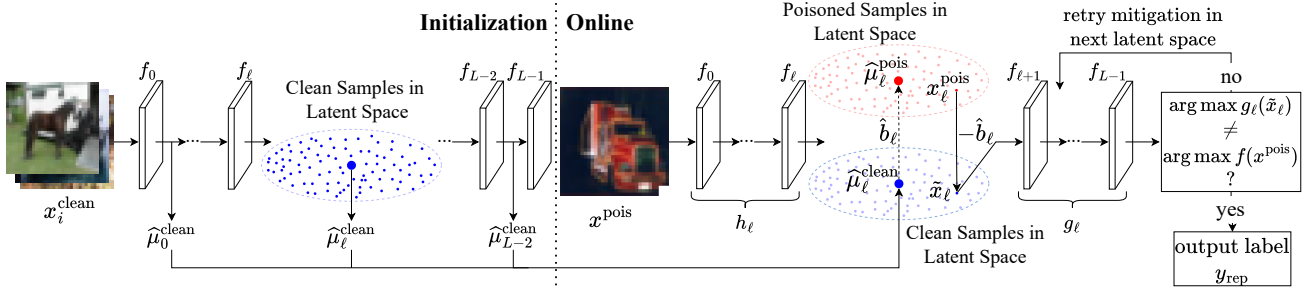


Figure 2. Overview of the defense procedure: The left side shows the short initialization phase, where a small set of clean samples is used to obtain the centroids $\hat{\mu}_\ell^{\text{clean}}$ in candidate latent spaces. The right side shows the online phase, where it is used to repair the latent representation of poisoned samples.

dition. The defense returns the output label of the earliest mitigation attempt that alters the prediction; if no shift induces a change, it leaves the prediction unchanged. Because the trigger-direction estimates are updated continuously as the stream progresses, the defense improves over time and becomes progressively more effective as evidence accumulates in online estimates.

6. Experiments

6.1. Experimental Settings

Our implementation builds on BackdoorBench (Wu et al., 2025). We evaluate on the same configurations as in Section 4; additional details are provided in Appendix C. For our defense, we assume access to a small clean reference set and use $N_c = 100$ clean samples by default to compute clean statistics and to support direction estimation². Strategy 2, with color jitter and Gaussian blurring as augmentation techniques, is used to obtain the latent directions. Furthermore, we choose the mixing weight λ as 0.5 and the repair intensity parameter α as 1.

Lightweight inference-time methods that *correct* predictions (rather than rejecting inputs) are relatively rare. We therefore compare against the state-of-the-art approach that supports runtime prediction correction: ZIP (Shi et al., 2023) leverages diffusion-based purification and can correct predictions at test time, but incurs substantial computational cost.

6.2. Runtime Mitigation Performance

Fig. 3 shows that FIRE is particularly effective in the streaming setting: it updates its mitigation decision as additional poisoned samples arrive, leading to consistently improving PA over the stream. Across the full benchmark suite in Tab. 2, FIRE already outperforms ZIP in **9/21** settings at the first poisoned sample (Pos 1), and it outperforms ZIP

²See Appendix E for results with different N_c .

Algorithm 1 Runtime latent-space backdoor mitigation

```

Input: model  $f$ , candidate layer indices  $\mathcal{L}$ , clean set  $\mathcal{D}_{\text{clean}}$ , augmentation  $\mathcal{A}$ , mixing weight  $\lambda \in [0, 1]$ 
Compute  $\hat{\mu}_\ell^{\text{clean}}$  from  $\mathcal{D}_{\text{clean}}$  for all  $\ell \in \mathcal{L}$  (Eq. 11)
Initialize  $\hat{\mu}_\ell^{\text{pois}} \leftarrow 0, \hat{\mu}_\ell^{\text{pois}, \text{aug}} \leftarrow 0$  for all  $\ell \in \mathcal{L}$ 
Initialize counters  $n_\ell \leftarrow 0$  and shifts  $\hat{b}_\ell \leftarrow 0$  for all  $\ell \in \mathcal{L}$ 
for each incoming poisoned sample  $x_t^{\text{pois}}$  do
     $y \leftarrow \arg \max f(x_t^{\text{pois}})$ 
     $x_t^{\text{pois}, \text{aug}} \leftarrow \mathcal{A}(x_t^{\text{pois}})$ 
    for each  $\ell \in \mathcal{L}$  in ascending order do
         $x_{t, \ell}^{\text{pois}} \leftarrow h_\ell(x_t^{\text{pois}}), x_{t, \ell}^{\text{pois}, \text{aug}} \leftarrow h_\ell(x_t^{\text{pois}, \text{aug}})$ ,
         $n_\ell \leftarrow n_\ell + 1$ 
         $\hat{\mu}_\ell^{\text{pois}} \leftarrow \hat{\mu}_\ell^{\text{pois}} + \frac{1}{n_\ell} (x_{t, \ell}^{\text{pois}} - \hat{\mu}_\ell^{\text{pois}})$ 
         $\hat{\mu}_\ell^{\text{pois}, \text{aug}} \leftarrow \hat{\mu}_\ell^{\text{pois}, \text{aug}} + \frac{1}{n_\ell} (x_{t, \ell}^{\text{pois}, \text{aug}} - \hat{\mu}_\ell^{\text{pois}, \text{aug}})$ 
         $\hat{b}_\ell \leftarrow \lambda(\hat{\mu}_\ell^{\text{pois}} - \hat{\mu}_\ell^{\text{clean}}) + (1 - \lambda)(\hat{\mu}_\ell^{\text{pois}} - \hat{\mu}_\ell^{\text{pois}, \text{aug}})$ 
         $\tilde{x}_{t, \ell} \leftarrow \text{Rep}_\ell(x_{t, \ell}^{\text{pois}}, \hat{b}_\ell, 1)$ 
         $y_{\text{rep}} \leftarrow \arg \max g_\ell(\tilde{x}_{t, \ell})$ 
        if  $y_{\text{rep}} \neq y$  then
            Output  $y_{\text{rep}}$  and break
        end if
    end for
    If no layer changed the prediction, output  $y$ 
end for

```

in **all 21/21** settings by the 10th poisoned sample (Pos 10). This trend is also reflected in Fig. 3, where ZIP remains flat because it does not incorporate new poisoned samples, while FIRE steadily improves and converges to high PA.

6.3. Execution Time Analysis

In addition to mitigation effectiveness, practical test-time defenses must meet strict latency constraints. We therefore evaluate the execution time of FIRE and ZIP in a *streaming* setting, where samples arrive one after another and the defense is required to mitigate the input and output the cor-

Table 2. Benchmark results for the streaming scenario: Clean Accuracy (CA, %) and Poisoned Accuracy (PA, %, higher is better) without a defense, Poisoned Accuracy (PA, %) for the ZIP and *FIRE* approaches, and the Time in milliseconds (ms, lower is better) are reported.

CONFIGURATION	ATTACK	CA \uparrow	PA \uparrow	ZIP PA \uparrow	FIRE PA \uparrow		ZIP TIME \downarrow	FIRE TIME \downarrow	
					POS 1	POS 10		INIT.	ONLINE
PREACTRESNET18 CIFAR-10	BADNETS	91.86	5.27	27.19	22.56	86.22	1408.0	223.7	14.0
	BLENDDED	93.57	0.18	45.00	25.44	64.00	1403.3	222.0	12.1
	BLIND	80.20	0.40	0.55	3.78	69.78	1418.0	228.5	15.2
	BPP	91.07	0.39	63.24	29.44	78.22	1404.4	213.6	11.8
	FTROJAN	93.56	0.00	61.02	29.44	67.67	1398.6	220.4	12.0
	INPUTAWARE	91.29	2.54	40.23	24.56	72.11	1424.4	214.4	12.1
	WANET	91.24	3.90	33.63	17.56	71.44	1452.3	219.2	16.8
PREACTRESNET18 GTSRB	BADNETS	96.05	3.73	6.25	76.53	86.95	1460.6	225.8	11.7
	BLENDDED	97.06	0.27	31.25	34.61	61.89	1472.8	231.8	12.8
	BLIND	57.33	41.23	27.73	21.88	49.01	1504.3	225.5	11.5
	BPP	96.80	0.24	69.92	85.28	82.66	1485.9	228.2	11.7
	FTROJAN	98.12	0.00	67.58	79.16	76.37	1494.6	241.0	12.0
	INPUTAWARE	97.53	6.17	50.39	71.20	61.89	1531.6	232.6	12.2
	WANET	96.79	7.06	31.25	20.29	42.32	1474.9	226.2	14.2
PREACTRESNET34 CIFAR-10	BADNETS	92.46	4.31	24.80	26.78	88.67	1449.7	208.5	22.1
	BLENDDED	94.02	0.21	45.66	26.89	61.78	1454.3	205.5	20.4
	BLIND	89.43	0.03	0.74	19.78	78.44	1398.4	212.1	24.2
	BPP	92.23	0.28	63.40	25.44	71.11	1407.8	209.4	21.8
	FTROJAN	93.63	0.06	62.34	29.11	82.89	1433.4	210.8	21.1
	INPUTAWARE	91.61	3.71	52.19	21.11	71.33	1409.6	221.1	23.2
	WANET	90.17	9.74	12.46	13.33	50.78	1409.5	209.5	26.2

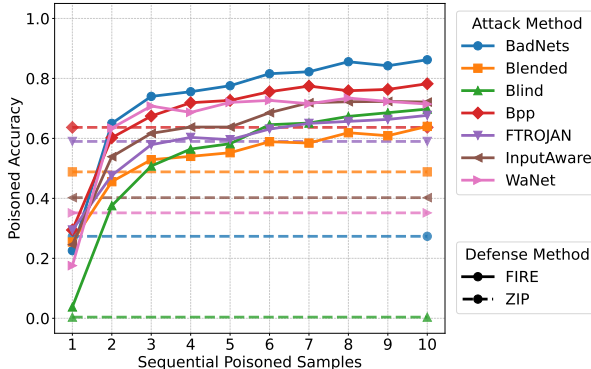


Figure 3. Runtime mitigation performance on CIFAR-10 with a PreActResNet18 using strategy 2 under a stream of poisoned samples. The x-axis denotes the poisoned sample index (arrival order), and the y-axis shows Poisoned Accuracy (PA, %). FIRE improves as additional poisoned samples arrive, whereas ZIP (dashed) remains constant because it does not adapt using new samples.

rected label as quickly as possible. All timing measurements were obtained on a single NVIDIA A100 GPU.

The right side of Tab. 2 summarizes the runtime results. After a brief initialization of around \sim 200–250 ms, FIRE enables consistently fast online processing across architectures, datasets, and attacks: it processes a sample in roughly **~11–27 ms**, while ZIP requires about \sim 1.4–1.6 s per sam-

ple. This \approx two-order-of-magnitude speedup makes FIRE well-suited for low-latency streaming inference, where real-time mitigation is essential.

7. Conclusion and Limitations

We analyzed backdoor behavior through intermediate representations and found that inspecting *multiple* latent spaces of a poisoned model can reveal where the trigger effect becomes structured, and thus exploitable for mitigation. Across a diverse set of attacks, datasets, and architectures, there is typically at least one latent space in which the trigger manifests as a *single, label-agnostic direction*, enabling reliable removal of the trigger component and recovery of the sample’s original label. Building on this observation, we introduced FIRE (*Feature-space Inference-time REpair*), a lightweight runtime defense that repairs latent representations during a forward pass by estimating a backdoor direction and subtracting its component at an appropriate layer, without retraining or changing model parameters. Experiments show strong label recovery that improves as more poisoned samples are processed in a stream, while incurring substantially lower overhead than prior runtime correction baselines. At the same time, our evaluation is currently limited to image models; extending FIRE to other domains (e.g., text or graphs) and to multi-objective backdoors that may require multiple shifts (possibly in multiple latent spaces) remains an important direction for future work.

8. Impact Statement

This paper presents work whose goal is to advance the field of Machine Learning. There are many potential societal consequences of our work. However, it aims to improve the security of machine learning model usage, which benefits the community.

References

Al Kader Hammoud, H. A., Bibi, A., Torr, P. H., and Ghanem, B. Don't FREAK Out: A Frequency-Inspired Approach to Detecting Backdoor Poisoned Samples in DNNs. *2023 IEEE/CVF Conference on Computer Vision and Pattern Recognition Workshops (CVPRW)*, pp. 2338–2345, June 2023. doi: 10.1109/CVPRW59228.2023.00230.

Bagdasaryan, E. and Shmatikov, V. Blind Backdoors in Deep Learning Models. In *30th USENIX Security Symposium (USENIX Security 21)*, pp. 1505–1521, 2021.

Bagdasaryan, E., Veit, A., Hua, Y., Estrin, D., and Shmatikov, V. How To Backdoor Federated Learning. In *Proceedings of the Twenty Third International Conference on Artificial Intelligence and Statistics*, pp. 2938–2948. PMLR, June 2020.

Bank, D., Koenigstein, N., and Giryes, R. Autoencoders. In Rokach, L., Maimon, O., and Shmueli, E. (eds.), *Machine Learning for Data Science Handbook*, pp. 353–374. Springer International Publishing, Cham, 2023. doi: 10.1007/978-3-031-24628-9_16.

Chen, X., Liu, C., Li, B., Lu, K., and Song, D. Targeted Backdoor Attacks on Deep Learning Systems Using Data Poisoning, December 2017.

Chen, Y., Shao, S., Huang, E., Li, Y., Chen, P.-Y., Qin, Z., and Ren, K. REFINE: Inversion-Free Backdoor Defense via Model Reprogramming. 2025. doi: 10.48550/ARXIV.2502.18508.

Cheng, S., Shen, G., Zhang, K., Tao, G., An, S., Guo, H., Ma, S., and Zhang, X. UNIT: Backdoor Mitigation via Automated Neural Distribution Tightening. In *European Conference on Computer Vision*. arXiv, 2024. doi: 10.48550/ARXIV.2407.11372.

Chou, E., Tramer, F., and Pellegrino, G. SentiNet: Detecting Localized Universal Attacks Against Deep Learning Systems. *2020 IEEE Security and Privacy Workshops (SPW)*, pp. 48–54, May 2020. doi: 10.1109/SPW50608.2020.00025.

Doan, B. G., Abbasnejad, E., and Ranasinghe, D. C. Februus: Input Purification Defense Against Trojan Attacks on Deep Neural Network Systems. In *Annual Computer Security Applications Conference*, pp. 897–912, December 2020. doi: 10.1145/3427228.3427264.

Gao, Y., Xu, C., Wang, D., Chen, S., Ranasinghe, D. C., and Nepal, S. STRIP: A Defence Against Trojan Attacks on Deep Neural Networks. *Proceedings of the 35th Annual Computer Security Applications Conference*, pp. 113–125, December 2019. doi: 10.1145/3359789.3359790.

Gao, Y., Chen, H., Sun, P., Li, Z., Li, J., and Shao, H. Energy-based Backdoor Defense without Task-Specific Samples and Model Retraining. In *Proceedings of the 41st International Conference on Machine Learning*, pp. 14611–14637. PMLR, July 2024.

Gu, T., Dolan-Gavitt, B., and Garg, S. BadNets: Identifying Vulnerabilities in the Machine Learning Model Supply Chain, March 2019a.

Gu, T., Liu, K., Dolan-Gavitt, B., and Garg, S. BadNets: Evaluating Backdooring Attacks on Deep Neural Networks. *IEEE Access*, 7:47230–47244, 2019b. ISSN 2169-3536. doi: 10.1109/ACCESS.2019.2909068.

Guo, J., Li, Y., Chen, X., Guo, H., Sun, L., and Liu, C. SCALE-UP: An Efficient Black-box Input-level Backdoor Detection via Analyzing Scaled Prediction Consistency. In *The Eleventh International Conference on Learning Representations*, September 2022.

He, K., Zhang, X., Ren, S., and Sun, J. Identity Mappings in Deep Residual Networks. In Leibe, B., Matas, J., Sebe, N., and Welling, M. (eds.), *Computer Vision – ECCV 2016*, volume 9908, pp. 630–645. Springer International Publishing, Cham, 2016. doi: 10.1007/978-3-319-46493-0_38.

Hu, T., Chen, F., Wang, H., Li, J., Wang, W., Sun, J., and Li, Z. Complexity Matters: Rethinking the Latent Space for Generative Modeling. In *Proceedings of the 37th International Conference on Neural Information Processing Systems, NIPS '23*, pp. 29558–29579, Red Hook, NY, USA, December 2023. Curran Associates Inc.

Huang, H., Wang, Q., Gong, X., and Wang, T. Orion: Online Backdoor Sample Detection via Evolution Deviance. In *Proceedings of the Thirty-Second International Joint Conference on Artificial Intelligence*, pp. 864–874, Macau, SAR China, August 2023. International Joint Conferences on Artificial Intelligence Organization. doi: 10.24963/ijcai.2023/96.

Jebreel, N. M., Domingo-Ferrer, J., and Li, Y. Defending Against Backdoor Attacks by Layer-wise Feature Analysis. In *Thirty-Third International Joint Conference on Artificial Intelligence*, volume 9, pp. 8416–8420, August 2024. doi: 10.24963/ijcai.2024/933.

Jin, L.-X., Jiang, W., Wen, X.-Y., Lin, M.-Y., Zhan, J.-Y., Zhou, X.-Z., Habtie, M. A., and Werghi, N. A survey of backdoor attacks and defences: From deep neural networks to large language models. *Journal of Electronic Science and Technology*, 23(3):100326, September 2025. ISSN 1674-862X. doi: 10.1016/j.jnest.2025.100326.

Krizhevsky, A. and Hinton, G. Learning multiple layers of features from tiny images. 2009.

Krizhevsky, A., Sutskever, I., and Hinton, G. E. ImageNet Classification with Deep Convolutional Neural Networks. In *Advances in Neural Information Processing Systems*, volume 25. Curran Associates, Inc., 2012.

Kurita, K., Michel, P., and Neubig, G. Weight Poisoning Attacks on Pretrained Models. In Jurafsky, D., Chai, J., Schluter, N., and Tetreault, J. (eds.), *Proceedings of the 58th Annual Meeting of the Association for Computational Linguistics*, pp. 2793–2806, Online, July 2020. Association for Computational Linguistics. doi: 10.18653/v1/2020.acl-main.249.

Li, X., Xiang, Z., Miller, D. J., and Kesidis, G. Backdoor Mitigation by Correcting the Distribution of Neural Activations, August 2023.

Li, Y., Lyu, X., Koren, N., Lyu, L., Li, B., and Ma, X. Neural Attention Distillation: Erasing Backdoor Triggers from Deep Neural Networks. In *International Conference on Learning Representations*, October 2020.

Li, Y., Zhai, T., Jiang, Y., Li, Z., and Xia, S.-T. Backdoor Attack in the Physical World, April 2021.

Li, Y., Zhu, C., Zhao, Y., and Zhang, J. BDFirewall: Towards Effective and Expeditiously Black-Box Backdoor Defense in MLaaS, August 2025.

Li, Y., He, J., Huang, H., Sun, J., Ma, X., and Jiang, Y.-G. Shortcuts Everywhere and Nowhere: Exploring Multi-Trigger Backdoor Attacks. *IEEE Transactions on Dependable and Secure Computing*, 23(1):343–355, January 2026. ISSN 1545-5971, 1941-0018, 2160-9209. doi: 10.1109/TDSC.2025.3605597.

Litjens, G., Kooi, T., Bejnordi, B. E., Setio, A. A. A., Ciompi, F., Ghafoorian, M., van der Laak, J. A. W. M., van Ginneken, B., and Sánchez, C. I. A survey on deep learning in medical image analysis. *Medical Image Analysis*, 42:60–88, December 2017. ISSN 1361-8415. doi: 10.1016/j.media.2017.07.005.

Liu, K., Dolan-Gavitt, B., and Garg, S. Fine-Pruning: Defending Against Backdooring Attacks on Deep Neural Networks. *Research in Attacks, Intrusions, and Defenses*, 11050:273–294, 2018. doi: 10.1007/978-3-030-00470-5-13.

Luo, S., Fan, X., Jing, Q., Lin, C., Li, M., Lu, Y., and Xu, Y. SifterNet: A Generalized and Model-Agnostic Trigger Purification Approach, May 2025.

May, B. B., Tatro, N. J., Walker, D., Kumar, P., and Shnidman, N. Salient Conditional Diffusion for Defending Against Backdoor Attacks, May 2023.

Mengara, O., Avila, A., and Falk, T. H. Backdoor Attacks to Deep Neural Networks: A Survey of the Literature, Challenges, and Future Research Directions. *IEEE Access*, 12:29004–29023, 2024. ISSN 2169-3536. doi: 10.1109/ACCESS.2024.3355816.

Mienye, E., Jere, N., Obaido, G., Mienye, I. D., and Aruleba, K. Deep Learning in Finance: A Survey of Applications and Techniques. *AI*, 5(4):2066–2091, December 2024. ISSN 2673-2688. doi: 10.3390/ai5040101.

Nguyen, T. A. and Tran, A. Input-Aware Dynamic Backdoor Attack. In *Advances in Neural Information Processing Systems*, volume 33, pp. 3454–3464. Curran Associates, Inc., 2020a.

Nguyen, T. A. and Tran, A. T. WaNet - Imperceptible Warping-based Backdoor Attack. In *International Conference on Learning Representations*, October 2020b.

Parihar, R., Dhiman, A., Karmali, T., and Babu, R. V. Everything is There in Latent Space: Attribute Editing and Attribute Style Manipulation by StyleGAN Latent Space Exploration. In *Proceedings of the 30th ACM International Conference on Multimedia*, pp. 1828–1836, October 2022. doi: 10.1145/3503161.3547972.

Shi, Y., Du, M., Wu, X., Guan, Z., Sun, J., and Liu, N. Black-box Backdoor Defense via Zero-shot Image Purification. In Oh, A., Naumann, T., Globerson, A., Saenko, K., Hardt, M., and Levine, S. (eds.), *Advances in Neural Information Processing Systems 36: Annual Conference on Neural Information Processing Systems 2023, NeurIPS 2023, New Orleans, LA, USA, December 10 - 16, 2023*, 2023.

Simonyan, K., Vedaldi, A., and Zisserman, A. Deep Inside Convolutional Networks: Visualising Image Classification Models and Saliency Maps. In *2nd International Conference on Learning Representations, ICLR 2014, Banff, AB, Canada, April 14-16, 2014, Workshop Track Proceedings*, 2014.

Stallkamp, J., Schlipsing, M., Salmen, J., and Igel, C. The German Traffic Sign Recognition Benchmark: A multi-class classification competition. In *The 2011 International Joint Conference on Neural Networks*, pp. 1453–1460, San Jose, CA, USA, July 2011. IEEE. doi: 10.1109/IJCNN.2011.6033395.

Sun, T., Pang, L., Lyu, W., Chen, C., and Ling, H. Mask and Restore: Blind Backdoor Defense at Test Time with Masked Autoencoder, August 2025.

Tampuu, A., Matiisen, T., Semikin, M., Fishman, D., and Muhammad, N. A Survey of End-to-End Driving: Architectures and Training Methods. *IEEE Transactions on Neural Networks and Learning Systems*, 33 (4):1364–1384, April 2022. ISSN 2162-2388. doi: 10.1109/TNNLS.2020.3043505.

Turner, A., Tsipras, D., and Madry, A. Label-Consistent Backdoor Attacks, December 2019.

Usman, M., Gopinath, D., Sun, Y., Noller, Y., and Pasareanu, C. NNRepair: Constraint-based Repair of Neural Network Classifiers, June 2021.

Usman, M., Gopinath, D., Sun, Y., and Păsăreanu, C. S. Rule-Based Runtime Mitigation Against Poison Attacks on Neural Networks. In *Runtime Verification: 22nd International Conference, RV 2022, Tbilisi, Georgia, September 28–30, 2022, Proceedings*, pp. 67–84, Berlin, Heidelberg, September 2022. Springer-Verlag. doi: 10.1007/978-3-031-17196-3_4.

Wang, B., Yao, Y., Shan, S., Li, H., Viswanath, B., Zheng, H., and Zhao, B. Y. Neural Cleanse: Identifying and Mitigating Backdoor Attacks in Neural Networks. In *2019 IEEE Symposium on Security and Privacy (SP)*, pp. 707–723, May 2019. doi: 10.1109/SP.2019.00031.

Wang, H., Xiang, Z., Miller, D. J., and Kesidis, G. Improved activation clipping for universal backdoor mitigation and test-time detection. In *2024 IEEE 34th International Workshop on Machine Learning for Signal Processing (MLSP)*, pp. 1–6. IEEE, 2024.

Wang, T., Yao, Y., Xu, F., An, S., Tong, H., and Wang, T. An Invisible Black-Box Backdoor Attack Through Frequency Domain. In Avidan, S., Brostow, G., Cissé, M., Farinella, G. M., and Hassner, T. (eds.), *Computer Vision – ECCV 2022*, pp. 396–413, Cham, 2022a. Springer Nature Switzerland. doi: 10.1007/978-3-031-19778-9_23.

Wang, T., Zhang, X., Jin, Y., Chen, C., and Zhu, F. Patch-Based Backdoors Detection and Mitigation with Feature Masking. In Chen, X., Huang, X., and Kutyłowski, M. (eds.), *Security and Privacy in Social Networks and Big Data*, pp. 229–246, Singapore, 2022b. Springer Nature. doi: 10.1007/978-981-19-7242-3_15.

Wang, Z., Zhai, J., and Ma, S. BppAttack: Stealthy and Efficient Trojan Attacks against Deep Neural Networks via Image Quantization and Contrastive Adversarial Learning. *2022 IEEE/CVF Conference on Computer Vision and Pattern Recognition (CVPR)*, pp. 15054–15063, June 2022c. doi: 10.1109/CVPR52688.2022.01465.

Wei, Y., Gao, H., Wang, Y., Gao, Y., and Liu, H. A lightweight backdoor defense framework based on image inpainting. *Neurocomputing*, 537:22–36, June 2023. ISSN 0925-2312. doi: 10.1016/j.neucom.2023.03.052.

Wu, B., Chen, H., Zhang, M., Zhu, Z., Wei, S., Yuan, D., Zhu, M., Wang, R., Liu, L., and Shen, C. BackdoorBench: A Comprehensive Benchmark and Analysis of Backdoor Learning. *International Journal of Computer Vision*, 133 (8):5700–5787, August 2025. ISSN 1573-1405. doi: 10.1007/s11263-025-02447-x.

Wu, B., Zhu, M., Zheng, M., Zhu, Z., Wei, S., Zhang, M., Chen, H., Yuan, D., Liu, L., and Liu, Q. Defenses in Adversarial Machine Learning: A Systematic Survey From the Lifecycle Perspective. *IEEE Transactions on Pattern Analysis and Machine Intelligence*, 48(1):876–895, January 2026. ISSN 1939-3539. doi: 10.1109/TPAMI.2025.3611340.

Xi, Z., Pang, R., Ji, S., and Wang, T. Graph Backdoor. In *30th USENIX Security Symposium (USENIX Security 21)*, pp. 1523–1540, 2021.

Xu, J., Ma, M., Wang, F., Xiao, C., and Chen, M. Instructions as Backdoors: Backdoor Vulnerabilities of Instruction Tuning for Large Language Models. In Duh, K., Gomez, H., and Bethard, S. (eds.), *Proceedings of the 2024 Conference of the North American Chapter of the Association for Computational Linguistics: Human Language Technologies (Volume 1: Long Papers)*, pp. 3111–3126, Mexico City, Mexico, June 2024. Association for Computational Linguistics. doi: 10.18653/v1/2024.naacl-long.171.

Xu, X., Huang, K., Li, Y., Qin, Z., and Ren, K. Towards Reliable and Efficient Backdoor Trigger Inversion via Decoupling Benign Features. In *The Twelfth International Conference on Learning Representations*, October 2023.

Yang, Y., Jia, C., Yan, D., Hu, M., Li, T., Xie, X., Wei, X., and Chen, M. SampDetox: Black-box Backdoor Defense via Perturbation-based Sample Detoxification. *Advances in Neural Information Processing Systems*, 37: 121236–121264, December 2024.

Zeiler, M. D. and Fergus, R. Visualizing and Understanding Convolutional Networks. In Fleet, D., Pajdla, T., Schiele, B., and Tuytelaars, T. (eds.), *Computer Vision – ECCV 2014*, pp. 818–833, Cham, 2014. Springer International Publishing. doi: 10.1007/978-3-319-10590-1_53.

Zeng, Y., Pan, M., Just, H. A., Lyu, L., Qiu, M., and Jia, R. Narcissus: A Practical Clean-Label Backdoor Attack with Limited Information. In *Proceedings of the 2023 ACM SIGSAC Conference on Computer and Communications Security, CCS '23*, pp. 771–785, New York, NY, USA,

November 2023. Association for Computing Machinery.
doi: 10.1145/3576915.3616617.

Zhai, T., Li, Y., Zhang, Z., Wu, B., Jiang, Y., and Xia, S.-T. Backdoor Attack Against Speaker Verification. In *ICASSP 2021 - 2021 IEEE International Conference on Acoustics, Speech and Signal Processing (ICASSP)*, pp. 2560–2564, June 2021. doi: 10.1109/ICASSP39728.2021.9413468.

Zhu, M., Wei, S., Zha, H., and Wu, B. Neural Polarizer: A Lightweight and Effective Backdoor Defense via Purifying Poisoned Features. *Advances in Neural Information Processing Systems*, 36:1132–1153, December 2023.

Zhu, M., Wei, S., Zha, H., and Wu, B. Class-Conditional Neural Polarizer: A Lightweight and Effective Backdoor Defense by Purifying Poisoned Features, February 2025.

A. Additional Strategies for Estimating the Trigger Direction

FIRE using augmentations only Rather than relying on representations extracted from clean samples, the method can be formulated entirely in terms of image augmentations. Under this formulation, the initialization step, namely the computation of the clean centroid, is no longer required. Alg. 2 presents this augmentation based variant.

Fig. 4a reports the performance when using FIRE using only image augmentations. As the number of samples increases, accuracy consistently improves, and even without additional techniques the model attains strong performance. While combining methods in Fig. 3 yields the better results, FIRE with augmentations alone already provides a solid and effective baseline.

Projection-based Repair If clean data is available, there is also the option of replacing the pure shift with a projection. For a given sample, it removes only the component of x_ℓ that lies along the augmentation-based direction \hat{b}_ℓ by projecting

Algorithm 2 Runtime latent-space backdoor mitigation using augmentations only

```

Input: model  $f$ , candidate layers  $\mathcal{L}$ , augmentation  $\mathcal{A}$ 
 $\hat{\mu}_\ell^{\text{pois,aug}} \leftarrow 0$  for all  $\ell \in \mathcal{L}$ 
Initialize counters  $n_\ell \leftarrow 0$  and shifts  $\hat{b}_\ell \leftarrow 0$  for all  $\ell \in \mathcal{L}$ 
for each incoming poisoned sample  $x_t^{\text{pois}}$  do
     $y \leftarrow \arg \max f(x_t^{\text{pois}})$ 
     $x_t^{\text{pois,aug}} \leftarrow \mathcal{A}(x_t^{\text{pois}})$ 
    for each  $\ell \in \mathcal{L}$  in ascending order do
         $x_{t,\ell}^{\text{pois}} \leftarrow h_\ell(x_t^{\text{pois}})$ ,  $x_{t,\ell}^{\text{pois,aug}} \leftarrow h_\ell(x_t^{\text{pois,aug}})$ ,  $n_\ell \leftarrow n_\ell + 1$ 
         $\hat{\mu}_\ell^{\text{pois}} \leftarrow \hat{\mu}_\ell^{\text{pois}} + \frac{1}{n_\ell} (x_{t,\ell}^{\text{pois}} - \hat{\mu}_\ell^{\text{pois}})$ 
         $\hat{\mu}_\ell^{\text{pois,aug}} \leftarrow \hat{\mu}_\ell^{\text{pois,aug}} + \frac{1}{n_\ell} (x_{t,\ell}^{\text{pois,aug}} - \hat{\mu}_\ell^{\text{pois,aug}})$ 
         $\hat{b}_\ell \leftarrow \hat{\mu}_\ell^{\text{pois}} - \hat{\mu}_\ell^{\text{pois,aug}}$ 
         $\tilde{x}_{t,\ell} \leftarrow \text{Rep}_\ell(x_{t,\ell}^{\text{pois}}, \hat{b}_\ell, 1)$ 
         $y_{\text{rep}} \leftarrow \arg \max g_\ell(\tilde{x}_{t,\ell})$ 
        if  $y_{\text{rep}} \neq y$  then
            Output  $y_{\text{rep}}$  and break
        end if
    end for
    If no layer changed the prediction, output  $y$ 
end for

```

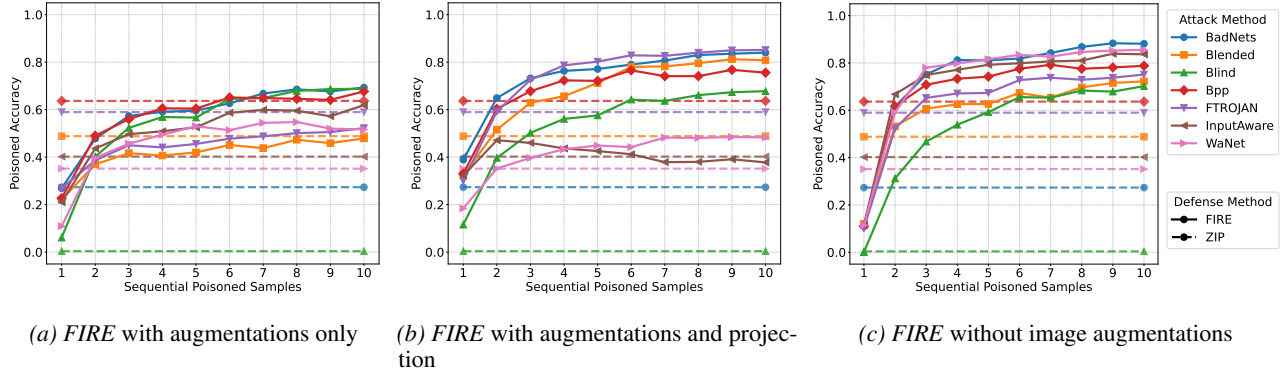


Figure 4. Mitigation performance on CIFAR-10 when using a PreActResNet18

Algorithm 3 Runtime latent-space backdoor mitigation without augmentations

Input: model f , candidate layers \mathcal{L} , clean set $\mathcal{D}_{\text{clean}}$
 Compute $\hat{\mu}_\ell^{\text{clean}}$ from $\mathcal{D}_{\text{clean}}$ for all $\ell \in \mathcal{L}$ (Eq. 11)
 Initialize $\hat{\mu}_\ell^{\text{pois}} \leftarrow 0$ for all $\ell \in \mathcal{L}$
 Initialize counters $n_\ell \leftarrow 0$ and shifts $\hat{b}_\ell \leftarrow 0$ for all $\ell \in \mathcal{L}$
for each incoming poisoned sample x_t^{pois} **do**
 $y \leftarrow \arg \max f(x_t^{\text{pois}})$
for each $\ell \in \mathcal{L}$ in ascending order **do**
 $x_{t,\ell}^{\text{pois}} \leftarrow h_\ell(x_t^{\text{pois}})$, $n_\ell \leftarrow n_\ell + 1$
 $\hat{\mu}_\ell^{\text{pois}} \leftarrow \hat{\mu}_\ell^{\text{pois}} + \frac{1}{n_\ell} (x_{t,\ell}^{\text{pois}} - \hat{\mu}_\ell^{\text{pois}})$
 $\hat{b}_\ell \leftarrow \hat{\mu}_\ell^{\text{pois}} - \hat{\mu}_\ell^{\text{clean}}$
 $\tilde{x}_{t,\ell} \leftarrow \text{Rep}_\ell(x_{t,\ell}^{\text{pois}}, \hat{b}_\ell, 1)$
 $y_{\text{rep}} \leftarrow \arg \max g_\ell(\tilde{x}_{t,\ell})$
if $y_{\text{rep}} \neq y$ **then**
Output y_{rep} and **break**
end if
end for
 If no layer changed the prediction, **output** y
end for

onto the affine subspace orthogonal to \hat{b}_ℓ around the clean centroid $\hat{\mu}_\ell^{\text{clean}}$:

$$\tilde{x}_\ell = \text{Rep}_\ell^{\text{proj}}(x_\ell) := x_\ell - \frac{\langle x_\ell - \hat{\mu}_\ell^{\text{clean}}, \hat{b}_\ell \rangle}{\|\hat{b}_\ell\|_2^2} \hat{b}_\ell. \quad (20)$$

This projection based repair adjusts x_ℓ only along the estimated trigger direction \hat{b}_ℓ , removing the \hat{b}_ℓ aligned component of the displacement $x_\ell - \hat{\mu}_\ell^{\text{clean}}$. Equivalently, it maps x_ℓ to the unique point obtained by moving along \hat{b}_ℓ that is closest in Euclidean distance to the clean centroid $\hat{\mu}_\ell^{\text{clean}}$, while leaving all components orthogonal to \hat{b}_ℓ unchanged.

As shown in Fig. 4b, projection-based repair improves accuracy for several attacks (BadNets, FTROJAN, Blended), while its effectiveness is attack-dependent and can degrade performance for others (InputAware, WaNet).

FIRE without image augmentations Li et al. show that, when a backdoored network is trained with image augmentations, it can become invariant to these transformations (2021), which can reduce the effectiveness of augmentation based variants. Nevertheless, FIRE can also be applied without augmentations, as summarized in Alg. 3.

Without augmentations, estimating the repair direction from a single incoming sample yields a trivial estimate: the resulting direction is simply the vector from the clean centroid to that sample in latent space. Consequently, repairing the first sample shifts it directly to the clean centroid, and the resulting prediction becomes largely independent of the sample’s original position. This limitation is visible in Fig. 4c. In the Blind attack setting, the centroid is (incidentally) classified as the target class, which leads to a PA of 0 for the first repaired sample. As more samples are observed, however, the trigger direction can be approximated more reliably, and subsequent samples can be repaired meaningfully.

B. Comparison with ShrinkPad

Besides ZIP, we also evaluated ShrinkPad (Li et al., 2021). ShrinkPad is an input-space purification baseline that shrinks and pads the input image to disrupt potential trigger patterns.

Tab. 3 summarizes results in the streaming setting. Overall, ShrinkPad is consistently fast (online runtime of roughly 3–5 ms per image), but its PA varies substantially across attacks and datasets. In contrast, FIRE achieves markedly higher PA in most configurations, especially at *Pos 10*, indicating that the latent-space correction benefits from a longer observation window. This robustness comes with a higher online cost (about 12–26 ms) and an additional one-time initialization (about 205–241 ms), but remains practical for streaming deployment.

Table 3. Benchmark results for the streaming scenario: Clean Accuracy (CA, higher is better), Poisoned Accuracy (PA, higher is better) for the ShrinkPad and FIRE approaches, and the Time in milliseconds (ms, lower is better) are reported.

CONFIGURATION	ATTACK	NO DEFENSE		SHRINKPAD		FIRE		SHRINKPAD		FIRE	
		CA	PA	PA ↑	PA ↑		TIME ↓	ONLINE	TIME ↓	INIT.	ONLINE
					POS 1	POS 10					
PREACTRESNET18 CIFAR-10	BADNETS	91.86	5.27	67.43	22.56	86.22	3.0	223.7	14.0		
	BLENDDED	93.57	0.18	33.82	25.44	64.00	2.8	222.0	12.1		
	BLIND	80.20	0.40	26.94	3.78	69.78	2.9	228.5	15.2		
	BPP	91.07	0.39	75.86	29.44	78.22	3.1	213.6	11.8		
	FTROJAN	93.56	0.00	78.89	29.44	67.67	2.7	220.4	12.0		
	INPUTAWARE	91.29	2.54	62.41	24.56	72.11	3.0	214.4	12.1		
	WANET	91.24	3.90	65.63	17.56	71.44	2.9	219.2	16.8		
PREACTRESNET18 GTSRB	BADNETS	96.05	3.73	27.06	76.53	86.95	2.8	225.8	11.7		
	BLENDDED	97.06	0.27	4.14	34.61	61.89	2.8	231.8	12.8		
	BLIND	57.33	41.23	33.69	21.88	49.01	2.9	225.5	11.5		
	BPP	96.80	0.24	28.20	85.28	82.66	3.0	228.2	11.7		
	FTROJAN	98.12	0.00	91.73	79.16	76.37	3.0	241.0	12.0		
	INPUTAWARE	97.53	6.17	58.50	71.20	61.89	3.0	232.6	12.2		
	WANET	96.79	7.06	41.69	20.29	42.32	3.0	226.2	14.2		
PREACTRESNET34 CIFAR-10	BADNETS	92.46	4.31	64.20	26.78	88.67	5.0	208.5	22.1		
	BLENDDED	94.02	0.21	37.56	26.89	61.78	5.3	205.5	20.4		
	BLIND	89.43	0.03	48.64	19.78	78.44	5.0	212.1	24.2		
	BPP	92.23	0.28	65.51	25.44	71.11	5.2	209.4	21.8		
	FTROJAN	93.63	0.06	78.13	29.11	82.89	5.0	210.8	21.1		
	INPUTAWARE	91.61	3.71	59.36	21.11	71.33	5.0	221.1	23.2		
	WANET	90.17	9.74	49.66	13.33	50.78	4.9	209.5	26.2		

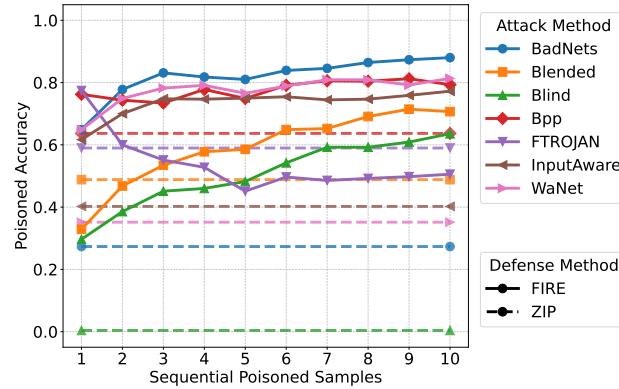


Figure 5. Mitigation performance on CIFAR-10 when using a PreActResNet18 when FIRE uses modified images generated by ShrinkPad as guidance.

Notably, there are a few cases where ShrinkPad matches or slightly exceeds FIRE (e.g., FTROJAN in several settings), suggesting that simple input transformations can be effective when the trigger is highly sensitive to resizing. However, across the broader benchmark, FIRE provides a more reliable PA improvement while maintaining competitive runtime.

Additionally, we evaluated ShrinkPad as an augmentation technique in combination with FIRE using Alg. 2. As shown in Fig. 5, for the first incoming poisoned sample the PA matches that of ShrinkPad alone, and for 6 out of 7 attacks performance improves as more examples are observed.

Table 4. Training details for each of the attacks: Number of training epochs (Epochs), Clean Accuracy (CA), Attack Success Rate (ASR), and Poisoned Accuracy (PA) are reported.

CONFIGURATION	ATTACK	EPOCHS	CA	ASR	PA
PREACTRESNET18 CIFAR-10	BADNETS	100	91.84	94.52	5.27
	BLENDED	100	93.57	99.81	0.18
	BLIND	100	80.17	99.59	0.40
	BPP	100	90.99	99.61	0.39
	FTROJAN	100	93.56	100.00	0.00
	INPUTAWARE	100	91.28	97.36	2.54
	WANET	100	91.19	95.83	3.90
PREACTRESNET18 GTSRB	BADNETS	50	96.05	96.13	3.73
	BLENDED	50	97.05	99.71	0.27
	BLIND	50	57.28	53.28	41.23
	BPP	50	96.79	99.76	0.24
	FTROJAN	50	98.11	100.00	0.00
	INPUTAWARE	50	97.51	93.38	6.17
	WANET	50	96.80	92.46	7.06
PREACTRESNET34 CIFAR-10	BADNETS	100	92.47	95.43	4.31
	BLENDED	100	94.04	99.79	0.21
	BLIND	100	89.36	99.97	0.03
	BPP	100	92.21	99.72	0.28
	FTROJAN	100	93.60	99.94	0.06
	INPUTAWARE	100	91.57	96.13	3.71
	WANET	100	90.15	89.67	9.74

C. Training Details for the Backdoored Models

Table 4 summarizes the training configurations and resulting performance metrics for the backdoored models used in Section 4 and 6. All models were trained following the default protocol and hyperparameter settings provided by Backdoor-Bench (Wu et al., 2025). For each attack, we report the number of training epochs (Epochs), CA, the attack success rate under the trigger (ASR), and PA.

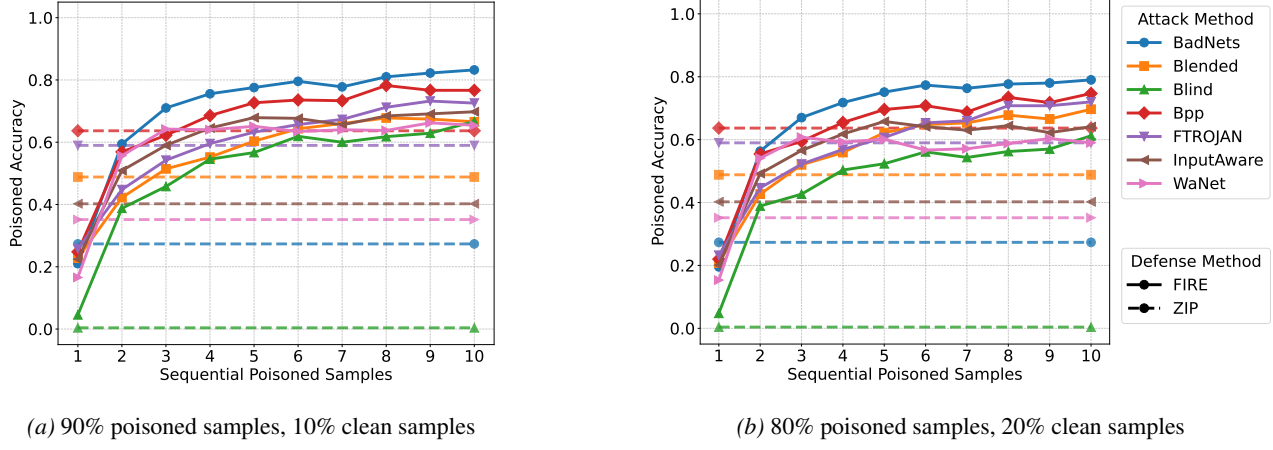
Overall, most attack configurations achieve high CA while attaining strong ASR, indicating effective backdoor implantation with limited degradation of clean performance. One notable exception is the Blind attack on GTSRB: the resulting model exhibits unusually low CA (57.28%) and comparatively low ASR (53.28%), alongside a markedly elevated PA (41.23%). This pattern suggests that the model did not converge to a well-performing solution under this configuration, i.e., Blind failed to train properly on GTSRB in our setting.

D. Impact of Imperfect Poisoned Sample Detection

In Section 5.1, we assume access to a stream of detected poisoned inputs that is provided to *FIRE*. In practice, however, any detector is likely to be imperfect and may occasionally misclassify clean samples as poisoned. We therefore evaluate how such false positives affect the mitigation performance of *FIRE*.

As illustrated in Fig. 6, increasing the fraction of incorrectly flagged clean samples leads to a gradual reduction in performance, as expected. Crucially, *FIRE* remains effective even under these imperfect conditions: across both settings, the method continues to mitigate the attack and maintains strong PA throughout the stream. Overall, these results indicate that *FIRE* is resilient to realistic detector noise and can still provide reliable protection when poisoned-sample detection is not fully accurate.

Tab. 5 complements this observation with a quantitative comparison. Even when the detector stream contains a non-trivial fraction of clean samples (90% / 80% poisoned), *FIRE* achieves PA that remains close to the standard setting in most cases. While some attacks incur moderate drops at Position 10 (e.g., BadNets and WaNet), others are largely unaffected, suggesting that *FIRE* does not critically depend on perfectly filtered inputs. On average, the PA at Position 10 decreases only by 1.22 points for the 90% setting and 4.25 points for the 80% setting, underscoring that *FIRE* continues to perform robustly under imperfect detection.



(a) 90% poisoned samples, 10% clean samples (b) 80% poisoned samples, 20% clean samples

Figure 6. Mitigation performance on CIFAR-10 when using a PreActResNet18 when the detection is imperfect.

Table 5. Benchmark results comparing FIRE performance with imperfect detectors. Poisoned Accuracy (PA, %) is reported at Position 1 and Position 10. Differences in PA at Position 10 are also shown.

CONFIGURATION	ATTACK	FIRE PA \uparrow		FIRE PA \uparrow (90%)		FIRE PA \uparrow (80%)		DIFFERENCE (POS 10)	
		POS 1	POS 10	POS 1	POS 10	POS 1	POS 10	0.9 - STD	0.8 - STD
PREACTRESNET18 CIFAR-10	BADNETS	22.56	86.22	21.00	83.22	19.56	79.00	-3.00	-7.22
	BLEND	25.44	64.00	22.78	66.56	20.78	69.67	2.56	5.67
	BLIND	3.78	69.78	4.56	66.67	4.78	61.22	-3.11	-8.56
	BPP	29.44	78.22	24.78	76.67	22.00	74.67	-1.55	-3.55
	FTROJAN	29.44	67.67	25.78	72.56	23.22	72.00	4.89	4.33
	INPUTAWARE	24.56	72.11	22.44	69.78	20.11	64.11	-2.33	-8.00
	WANET	17.56	71.44	16.56	65.44	15.33	59.00	-6.00	-12.44
AVERAGE		21.83	72.78	19.70	71.56	17.97	68.52	-1.22	-4.25

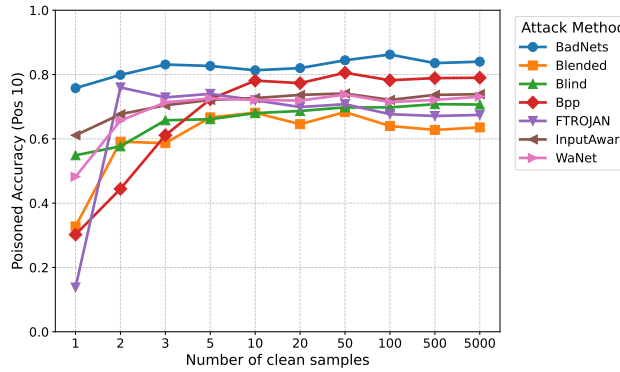


Figure 7. Poisoned accuracy for the 10th processed sample on CIFAR-10 using a PreActResNet18, as a function of the number of clean samples used to estimate the clean centroid.

E. Impact of the Number of Clean Samples on Direction Estimation

Fig. 7 reports the PA for the 10th processed sample as a function of the number of clean samples used to estimate the clean centroid. Even with very limited clean data, FIRE achieves competitive performance, and increasing the number of clean samples rapidly strengthens the centroid estimate. For most attacks, the PA stabilizes once roughly 10 clean samples are available, indicating that only a small clean set is sufficient in practice. Overall, these results highlight that FIRE is sample-efficient and remains effective when clean data access is constrained.